Article

Eco-friendly Synthesis from Industrial Wastewater of Fe and Cu Nanoparticles over NaX Zeolite and Activity in 4-Nitrophenol Reduction[†]

Amal Elfiad[1,2*], Daria Camilla Boffito[2], Sihem Khemassia[3], Federico Galli[2], Salah Chegrouche[3], Laaldja Meddour-Boukhobza[1].

[1]Laboratoire des Matériaux Catalytiques et Catalyse en Chimie Organique, Faculté de Chimie, USTHB, BP32 El Alia, Bab Ezzouar, 16111 Algiers, Algeria

[2]Department of Chemical Engineering, École Polytechnique de Montréal, Montreal, Quebec, Canada H3C3A7.

[3]Centre de Recherche Nucléaire de Draria, Commissariat à l'énergie Atomique, Alger, Algérie.

Corresponding Author: Amal Elfiad

*aelfiad@usthb.dz

[†]This article has been accepted for publication and undergone full peer review but has not been through the copyediting, typesetting, pagination and proofreading process, which may lead to differences between this version and the Version of Record. Please cite this article as doi: [10.1002/cjce.23083]

Additional Supporting Information may be found in the online version of this article.

Received 28 August 2017; Revised 5 October 2017; Accepted 11 October 2017
The Canadian Journal of Chemical Engineering

DOI 10.1002/cjce.23083

Abstract

We deposited Fe and Cu over zeolite NaX (Fe/NaX and Cu/NaX) by adsorption from effluent industrial wastewater. We synthesized the zeolite NaX by the hydrothermal method. 5 g of NaX adsorbed completely 350 and 380 mg of Fe and Cu from the industrial wastewater, respectively, in 6 h. The distribution of Fe and Cu over the NaX was uniform and amounted at 14 and 18 mass%, respectively. Fe and Cu modify the morphology of the NaX zeolite: the particle size increased from 9 μm to 10 μm for the former and decreased to 3 μm for the latter. Fe/NaX and Cu/NaX are less crystalline than NaX. BET analysis showed that the specific surface area decreased by 30 % and 50 % compared to NaX for Fe/NaX and Cu/NaX, but the ratio between meso- and micropores increased by 7 and 13 times, respectively. Fe/NaX and Cu/NaX synthesized by adsorption from industrial wastewater reduced +99 % of 4-p-nitrophenol to 4-aminophenol in less than 100 s, which is comparable to noble metal.

Keywords: Fe and Cu catalyst, industrial wastewater, adsorption, eco-friendly synthesis, 4-Nitrophenol.

INTRODUCTION

Dyes, pesticides, explosives and pharmaceutical industries release wastewater containing nitro-aromatic pollutants and metals.[1,2] Phenols carrying functionalities such as nitrile, nitrate, and chlorine are more toxic than phenols and anilines for both humans and wildlife. The aquatic ecotoxicity of 4-nitrophenol[3] ranges from slight to moderate and may affect growth, accumulation, mating, mortality, and feeding behavior among other factors.[4] When 4-nitrophenol (4-NP) comes in contact with the human body, it damages the skin, and the respiratory and digestive systems.[1,5–8] Due to its solubility and stability in water, the U.S Environmental Protection Agency has listed 4-NP among the most dangerous pollutants, limiting its concentration in water to 10 ppm.[8,9] The catalytic reduction of 4-NP to 4-aminophenol (4-AP) by $NaBH_4$ at room temperature may be of interest for those industrial processes whereby 4-AP is an intermediate, including pharmaceutical processes (for 4-AP derived analgesics, such as paracetamol and acetaminophen), as well as for the production of dyes, pigments, corrosion inhibitors, and anti-corrosion lubricants.[10] This reaction is common in literature over noble metal nanocatalysts, such as Au, Ag Pt, Pd,[11,12] or over Co.[13] Non-noble metals, though less active, are an alternative to the uneconomical and scarce noble metals. Up to now, metal nanoparticles (NPs) such as Cu, Al, Mg, Zn, and Fe and their oxides have been adopted for both liquid and gas phase reactions, either supported or unsupported. Examples of supports are zeolites, carbon, clay, metal oxides, graphene, etc. [13,14] Their applications include dye abatement in water,[13] organic synthesis,[14,15] water gas shift,[16] polymerization,[17] and photocatalysis.[18] Heavy metals in industrial wastewater represent another issue for the ecosystem,[19] in particular for the aquatic, due to their highly carcinogenic nature and their impossibility to be biodegraded.[15,16] Cu is one of the most widespread heavy metals in water.[20,21] It causes metabolic disorders,[22] and severe toxicological effects on humans and animals.[17] Together with Cu, Fe (III) is a common metal contained in tap water. It causes severe consequences over 60 mg/kg.[18] Moreover, excessive Fe in the blood damages the gastrointestinal tract.[14]

In the last few decades, reverse osmosis, flocculation,[23] bacterial action, ion exchange,[19] and adsorption processes[24,25] have been adopted to reduce heavy metals from waters and wastewaters. Among them, adsorption is the most efficient because of its simple design, low cost, and easy operation.[26]

NaX zeolite is largely used as an absorbent[27,28] and catalyst due its temperature stability, ion-exchange properties, and high porosity.[29,30]

NaX zeolite exchanged with Cu^{2+} absorbs toluene in gas phase[31] and Fe/NaX catalyzes the chemical vapour deposition synthesis of carbon nanotubes.[32] However, there are no literature data on the liquid-phase catalytic activity of Fe and Cu supported over NaX zeolite.

Here we report for the first time the synthesis of Fe/NaX and Cu/NaX via $Cu^{2+}$and Fe^{3+} adsorption contained in industrial wastewater and the test of their catalytic activity in the reduction of 4-NP to 4-AP.

Our work is original in several aspects: i) we are the first to report the synthesis of Fe/NaX and Cu/NaX from industrial wastewater; ii) we adopt for the first time non-noble metal catalysts for the reduction of 4-NP to 4-AP; iii) we test Fe and Cu-based zeolites in a liquid phase reaction; iv) the catalyst activity (> 99 % conversion in less than 100 s) is unprecedented in literature for the reduction of 4-NP to 4-AP.

EXPERIMENTAL

Effluent sample

The Observatory National of Environment and Development Durable (ONEDD) laboratory (Algeria) provided the industrial wastewater effluents (WE) samples.

The first effluent (WE-A) contained 350 mg/L of iron (Fe^{3+}) after the COD (chemical oxygen demand) test. Before the COD test, iron is not available in the solution: its concentration is lower than 10 ppm. The second effluent (WE-B) contained 400 mg/L of copper (Cu^{2+}) after the TKN test (Total Kjeldahl nitrogen). The same holds for the total nitrogen test. All copper was released after the test. Atomic adsorption spectroscopy (AAS) measured both the metals' concentrations (Table 1).

Zeolite NaX synthesis

Zeolite NaX was prepared by the hydrothermal method with 1.44 of Si/Al; the molar ratio composition of the gel was SiO_2/Al_2O_3 = 3.44, Na_2O/SiO_2 = 1.32 H_2O/ Na_2O = 38.80.[33] We purchased the precursors from Merck and used them without further purification.

We added a calculate amount of the aluminum (100 %, Merck) source to a NaOH (1.25 mol/L) solution (NaOH 98 %, Prolabo) and deionized water under agitation, and stirred continuously until all the aluminum had completely dissolved. After filtration, 6.88 g of sodium silicate (30 % SiO_2, 12 % Na_2O, 58 % H_2O, BDH) was added to the first solution until a homogeneous alumino-silicate gel formed. We kept the gel under stirring at room temperature for 24 h. Successively, we transferred the gel in a Teflon-lined stainless steel autoclave and kept it for 6

hours under autogenous pressure at 100 °C. The product was filtered, washed with deionized water until the pH = 7, and dried at 80 °C for 24 h. A furnace calcined the catalyst at 600 °C for 5 h, at a heating rate of 10 °C/min.

Fe/NaX and Cu/NaX zeolite synthesis

We evaluated the adsorption equilibrium of Fe and Cu on NaX zeolite at room temperature (25 ± 1 °C), at an initial concentration of metals of 350 mg/L and 400 mg/L respectively, in a 100 mL solution containing 0.4 g of zeolite. We prepared the solutions dissolving iron nitrate ($Fe(NO_3)_3 \cdot 9H_2O$) and copper nitrate ($Cu(NO_3)_2 \cdot 6H_2O$) in distilled water. We adjusted the pH with HNO_3 and NaOH 0.1 mol/L solutions to the desired value (Table 2). We stirred the suspensions at 300 rpm for 360 min. We separated the solid from the liquid by centrifugation at 4000 rpm for 15 min. We analyzed the liquid phase by AAS to quantify the Fe (III) and Cu (II).

We conducted some preliminary tests to identify the best adsorption conditions to remove Fe (III) and Cu (II), including initial pH, contact time, and adsorbent loading (all the experimental data are reported in the supplementary material). We only report the optimal adsorption conditions (Table 2), while in the adsorption tests the pH ranged from 1.5 to 4, the contact time ranged from 0.08–7 h, and the NaX loading ranged from 0.5 to 8 g per 100 mL Cu (II) and Fe (III) solutions.

We calculated the Cu and Fe percent adsorption as:

$$\% R = (C_0 - C_t) * 100 / C_0 \quad (1)$$

where C_0 (mg/L) is the initial Fe or Cu concentration (350 mg/L and 400 mg/L, respectively), and C_t (mg/L) is the concentration of metal ions in at time t.

After the evaluation of the optimum conditions (Table 2) with the synthetic solutions, we applied them on the real wastewater effluents (WE-A and WE-B, Table 1). The Fe and Cu ions absorbed entirely on NaX zeolite (Table 3). Other cations may be adsorbed, but their initial concentration is negligible compared to that of Fe^{3+} and Cu^{2+} (Table 1).

A centrifuge recovered the solids at 4000 rpm for 15 min. These were washed several times with deionized water until neutrality. The powders were dried at 130 °C for 12 h. The final zeolites are referred as to Fe/NaX and Cu/NaX.

Sample characterization

A SETARAM Labsys instrument for thermogravimetric and differential thermal analysis (TG/DTA) heated the samples in air at a rate of 10 °C/min from room temperature to 500 °C.

A Philips APD-3720 X-ray diffractometer collected the XRD patterns with a Cu Kα(λ = 0.154 nm) radiation. It operated in the 2θ range of 5–70° and identified the phase peaks by comparison with the PDF-ICDD (Powder Diffraction File International Center for Diffraction Data). A field emission scanning electron microscope (FE-SEM-JEOL JSM-7600F) with a voltage of 5 kV produced sample images. Scanning electron microscopy energy dispersive X-ray spectroscopy (SEM-EDS) detected the distribution of the elements. It operated at a voltage of 5 kV with an energy range of 10 keV.

An ORIBA LA-950 laser beam analyzer determined the particle size distribution (PSD) of the zeolites.

An autoadsrb-1 (Quantachrome) instrument measured the specific area, pore volume and pore size distribution of the samples by N_2 adsorption-desorption isotherms at 77 K. Fe and Cu concentrations were determined by atomic adsorption spectroscopy (AAS) (Shimadzu PERKIN-ELMER-2380). The error of AAS is lower than 0.1 %.

Catalytic activity

4-Nitrophenol (4-NP) reduced to 4-aminophenol (4-AP) over Fe/NaX and Cu/NaX in a standard quartz cell at 25 °C in the presence of an excess of $NaBH_4$. We tested NaX zeolite as a blank. 20 mL of 4-NP (5 mmol/L) were mixed with 12.5 mL of 0.5 mol/L aqueous solution of $NaBH_4$ and kept under stirring. After, 3 mL of this mixture were transferred in a quartz cell, 1 mg of the modified zeolite was added, and the solution (time zero) was quickly subjected to UV-vis to obtain the reaction kinetics. Catalysts were re-used 5 times to quantify their recyclability. At the end of each activity test, the catalyst was recovered by centrifugation and washed with distilled water. We studied 4-NP reduction kinetics by motioning the absorbance evolution after different intervals time with a UV-Vis spectrophotometer (JASCO model V-530) in the 250–500 nm range.

RESULTS AND DISCUSSION

Thermogravimetric analysis (TGA/DTA)

Before calcination, zeolite NaX lost about 0.21 g/g of its weight between room temperature and 200 °C, according to the DTA endothermic peaks at 55 and 143 °C (Figure 1, TGA/DTA curve). This corresponds to the loss of residual water and adsorbed water respectively.[34] Above 200 °C, no mass loss is observed, which confirms the formation of the final stable phase.

X-ray diffraction (XRD)

The XRD patterns of NaX (Figure 2a) and Fe/NaX, Cu/NaX (Figures 2b–c) reveal a similar diffraction behavior for all samples, which corresponds to the diffractogram of pure faujasitic zeolite X (PDF-ICDD 38–0237). This data are in agreement with those reported in the literature for the same powders.[35] The XRD did not detect any Cu or Fe containing phase, implying a homogeneous and fine distribution of Fe and Cu over the surface and in the pores. EDX analysis detected Cu and Fe on the catalysts' surface: 5.7 and 6.9 At %, respectively.

On the other side, after the incorporation of metals into the zeolite structure, NaX peak intensities decrease. This may be attributed to the reduction of the zeolite crystallite size,[36] along with non-uniformity of crystallite size as a consequence of the incorporation.[37]

Scanning Electron Microscopy (SEM)

The surface morphology and chemical composition of the Cu and Fe-modified zeolite samples were determined by SEM-EDS analysis (Figures 3a–c).

NaX zeolite exhibits a smooth surface with a cubic shape typical of faujasitic zeolite (zeolite X) (Figure 3a).[35] After Fe and Cu adsorption, the morphology of zeolite X changed. Fe/NaX surface morphology presents some irregularities, i.e. Fe acted as an abrasive (Figure 3b). This result may indicate that the iron ion did not adsorb in the zeolite matrix, but formed instead an "egg-shell" structure on the surface.[38] On the other hand, a smooth surface is observed for Cu/NaX zeolite (Figure 3c). Indeed, the Cu disperses homogeneously throughout zeolite structures.[39] SEM images of zeolites suggest that their morphology and particle size changed after adsorption. These results are in agreement with the data reported by Zhang et al., who exchanged zeolite NaX with Co.[36]

According to energy dispersive X-ray analysis (EDS), Fe and Cu are uniformly distributed over the NaX zeolite (Figure 4). Elemental mapping images proved the presence of Fe and Cu (Figure 4). The atomic and weight ratios are listed in Table 4. The Cu percentage is greater than Fe since WE-B contains 400 ppm of Cu, while Fe's concentration in WE-A is 350 ppm and both metals' adsorption is almost complete.

Particle size distribution (PSD)

After Fe and Cu adsorption, the PSD changed: NaX zeolite had an average particle size of 9 μm, while Fe/NaX and Cu/NaX had an average particle diameter of 10 μm and 3 μm, respectively. The PSD difference is ascribable to the incorporation and distribution of ions on

the NaX zeolite as outlined in the previous section. Fe/NaX exhibited a bimodal PSD with a secondary particle size of 110 µm, which can be attributed to the agglomeration of primary smaller particles.

Nitrogen adsorption measurement

We report the N_2 adsorption-desorption isotherms of NaX, Fe/NaX, and Cu/NaX in Figure 5 and summarize the textural properties of the samples in Table 4. The NaX isotherm (Figure 6) exhibits a type-I isotherm behavior according to IUPAC classification, confirming its microporous structure. The Cu/NaX, Fe/NaX samples are type I/II isotherms, and the hysteresis loop belongs to the H3 type. The results indicate that they possess a micropore-mesopore composite structure. The hysteresis of Fe/NaX and Cu/NaX indicate a developed mesoporosity compared with that of NaX.

Compared with pure zeolite NaX, the adsorption of the Fe and Cu decreases the BET surface area and pore volume, while the pore diameter significantly increases (Figure 4). The surface area of the zeolite samples follows the order NaX > Fe/NaX > Cu/NaX (Figure 4). Their reductions in SSA compared to the parent NaX are 30 and 50 %, respectively. Previous papers reported that when a metal is incorporated into the pores of the support, the surface area decreases due to the partial blocking of the zeolite pore by Fe and Cu ions, leading to a reduction of the total specific surface area.[37,40,41] This is confirmed by the decreased trend in the pore volume.[42] However, the increase in the pore radius ($V_{mesopore}$ versus $V_{micropore}$, Table 5) for Fe/NaX and Cu/NaX is caused by the enforced location of the metals species in the zeolite pores, leading to their enlargement. The X-ray diffractograms confirm this trend with a decrease in the crystallinity of Fe/NaX and Cu/NaX compared to NaX.[43]

Catalytic reduction of 4-nitrophenol

We selected the 4-nitrophenol (4-NP) reduction to 4-aminophenol (4-AP) in the presence of $NaBH_4$ as a model reaction to investigate the catalytic performance of Fe/NaX and Cu/NaX samples synthesized in-situ. This reaction yields one single product (4-AP) that absorbs at 300 nm.[44,45] 4-NP has a characteristic absorbance at 317 nm (Figure 7c) in neutral or acidic conditions.[46] After the addition of $NaBH_4$, the maximum adsorption shifts to 400 nm (Figure

7c), with a color change from light yellow to bright yellow, indicating the formation of 4-nitrophenolate ions in alkaline conditions.[47]

Even after several minutes, the maximum adsorption of p-nitrophenolate remained at 400 nm in the presence of $NaBH_4$, which confirms that the reduction does not proceed in aqueous $NaBH_4$ solution without a catalyst.[44] After the addition of the Fe/NaX and Cu/NaX , the color of the solution gradually changed from yellow to colourless, and the intensity of the strong adsorption peak at 400 nm gradually decreased. A new peak appeared at about 300 nm (Figure 6c), which corresponds to 4-AP.[48] An isosbestic point at 320 nm appeared in the UV–Vis spectra (Figure 7a–b), indicating that the catalytic reduction of 4-NP yields only 4-AP without by-products.[49] We added $NaBH_4$ in a larger excess compared to 4-NP concentration, so we can consider that its concentration remains constant during the reaction. Moreover, a $NaBH_4$ excess protects 4-AP from oxidation.[50]

The absorbance of 4-NP is proportional to its concentration in the medium, the A_t/A_0 ratio is proportional to the C_t/C_0 ratio. A_t is the absorbance at time t, A_0 is the absorbance at time t = 0, C_t is the concentration of 4-NP at the reaction time t and C_0 is the initial concentration of 4-NP. The pseudo-first order rate constant is calculated by the following equation:

$$-ln\ C_t/C_0 = ln(A_t/A_0) = -kt \quad (2)$$

where, k is the rate constant.

The plots of $\ln(A_t/A_0)$ versus time (t) for the 4-nitrophenolate reduction in the presence of the catalysts are shown in Figure 8. The higher the rate of reduction, the greater is the value of the rate constant (1/s). The rate constants obtained from the slope of the plot of $\ln(A_t/A_0)$ versus time (t) are 0.035 1/s (Fe/NaX) and 0.064 1/s (Cu/NaX). In the presence of Cu/NaX (Figure 9), 100 % of 4-nitrophenolate converts in the first 60 s, while over Fe/NaX, the reaction takes 100 s to complete.

In the case of NaX, the reaction took 2100 s to complete. This clearly indicates that zeolite only is not active and that the activity of Cu/NaX is higher than that of Fe/NaX.

In the reduction of 4-NP into 4-AP, metal particles catalyze the reduction by acting as an electronic system, where the active metal facilitates the electron transfer from the donor nucleophile BH_4^- to the acceptor nitro group.[51-53]

The catalytic reduction over Cu/NaX and Fe/NaX includes the following steps (Figure 11): (i) chemisorption of BH^-_4 on the Cu/NaX and Fe/NaX surface; (ii) the electron transfer from the donor BH^-_4 to the acceptor 4-NP occurs, whereby the Fe^{3+} and Cu^{2+} react with BH^-_4 forming a metal hydride complex that transfers surface hydrogen species (H) and electrons (e^-) to 4-NP;[54,55] (iii) two reduced intermediates, –NO and –NHOH (Figure 10),[56] form; (iv) 4-NO reduces to 4-AP; (v) 4-AP desorbs from the surface of the catalyst.[48,57] The reduction mechanism of 4-NP on Fe/NaX and Cu/NaX is illustrated in Figure 11.

The catalytic efficiency depends on the surface structure and electron transfer properties of the catalyst;[58] the high activity of Cu/NaX and Fe/NaX compared to NaX is related to the dispersion of Cu and Fe over the zeolite, which provides more accessible reactive sites for the reduction of 4-NP.[57] Moreover, the surface positive charge of zeolites facilitated the interaction between the surface and the donor species BH^-_4,[59] as well between zeolite and the metal.[48]

We explain the higher catalytic performance of Cu/NaX zeolite with the greater positive reduction potential (+0.34 V) for the Cu^{2+}/Cu couple in comparison with Fe^{3+}/Fe (−0.036 V), which in turn facilitates the mobility of the electrons to the 4-NP.[60]

We compared the efficiency of Cu and Fe supported over zeolite with other catalytic systems for the same reaction (Table 6). Our samples reached the maximum conversion faster than any other kind of catalyst. Furthermore, we employed only 1 mg of catalyst to achieve the full conversion.

Only Cu nanoparticles over bentonite[61] and $Cu/Cu_2O/C$[65] have comparable results with our samples. However, the advantage of the materials we propose lies in the inexpensive synthesis (we treat wastewaters to adsorb metals on our catalysts).

Catalyst re-uses

We recovered and re-used Fe/NaX and Cu/NaX 5 times. The catalysts are stable (Figure 12). The activity remained unchanged over the first 300 s. We ascribe the small loss (5 % after 5 runs) in the 4-NP conversion to the catalyst loss during the separation and washing procedures.

CONCLUSIONS

We synthesized Fe/NaX and Cu/NaX from industrial wastewater after optimizing the adsorption conditions for Fe and Cu cations. The distribution of Fe and Cu over NaX was uniform and amounted at 0.14 and 0.18 g/g respectively. This synthesis procedure is new, efficient, and environmentally friendly. The catalysts reduced 4-nitrophenol to 4-aminophenol at ambient temperature in the presence of $NaBH_4$. The reaction time to complete the conversion was 60 s and 100 s for Cu/NaX and Fe/NaX, respectively, which is unprecedented, even compared to the noble catalysts reported in the literature. Our work shows new opportunities for the NP's supported zeolite synthesis using wastewater adsorption treatment, and pollutant reduction with great environmental potential.

REFERENCES

[1] P. Yang, A.-D. Xu, J. Xia, J. He, H.-L. Xing, X.-M. Zhang, S.-Y. Wei, N.-N. Wang, *Appl. Catal., A-Gen.* **2014**, *470*, 89.
[2] T. Vincent, E. Guibal, *Langmuir* **2003**, *19*, 8475.
[3] F. O. T. Sagban, *J. Environ. Sci*. **2011**, *23*, 616.
[4] S. Kegley, B. Hill, S. Orme, A. Choi, "PAN Pesticide Database," *Pesticide Action Network*, **2014**, accessed on 10 September 2017, http://www.pesticideinfo.org.
[5] M. Miranzadeh, M. Z. Kassaee, *Chem. Eng. J*. **2014**, *257*, 105.
[6] C. Wang, H. Zhang, C. Feng, S. Gao, N. Shang, Z. Wang, *Catal. Commun*. **2015**, *72*, 29.
[7] B. Lai, Y. Zhang, Z. Chen, P. Yang, Y. Zhou, J. Wang, *Appl. Catal. B-Environ.* **2014**, *144*, 816.
[8] C. Du, S. He, X. Gao, W. Chen, *ChemCatChem*. **2016**, *8*, 2885.
[9] P. Jiang, J. Zhou, A. Zhang, Y. Zhong, *J. Environ. Sci*. **2010**, *22*, 500.
[10] W. Dong, S. Cheng, C. Feng, N. Shang, S. Gao, C. Wang, *Cat. Commun*. **2017**, *90*, 70.
[11] Y. Deng, Y. Cai, Z. Sun, J. Liu, C. Liu, J. Wei, W. Li, C. Liu, Y. Wang, D. Zhao, *J. Am. Chem. Soc*. **2010**, *132*, 8466.
[12] J. Ge, T. Huynh, Y. Hu, Y. Yin, *Nano Lett*. **2008**, *8*, 931.
[13] H. Chen, M. Yang, S. Tao, G. Chen, *Appl. Catal. B-Environ*. **2017**, *209*, 648.
[14] J. M. Sieliechi, G. J. Kayem, I. Sandu, *International Journal of Conservation Science* **2010**, *1*, 175.
[15] R. Wuana, F. Okieimen, J. Imborvungu, *Int. J. Environ. Sci. Te.* **2010**, *7*, 485.
[16] M. Shavandi, Z. Haddadian, M. Ismail, N. Abdullah, Z. Abidin, *J. Taiwan Inst. Chem. E*. **2012**, *4*, 750.
[17] S. Wang, T. Terdkiatburana, M. Tadé, *Sep. Purif. Technol.* **2008**, *62*, 64.
[18] M. El-Harbawi, A. Sabidi, E. Kamarudin, A. Hamid, S. Harun, A. Nazlan, C. Yi, *Journal of Engineering Science and Technology* **2010**, *5*, 165.
[19] K. Rida, W. Goutas, I. Medjetena, *Can. J. Chem. Eng*. **2012**, *90*, 1269.
[20] Q. Meng, H. Chen, J. Lin, Z. Lin, J. Sun, *J. Environ. Sci*. **2017**, *56*, 254.
[21] K. Khan, Y. Lu, H. Khan, S. Zakir, S. Khan, A. A. Khan, L. Wei, T. Wang, *J. Environ. Sci*. **2013**, *2*, 2003.
[22] S. Svilović, D. Rušić, R. Stipišić, *J. Hazard. Mater*. **2009**, *170*, 941.
[23] V. Golob, A. Vinder, M. Simonič, *Dyes Pigments* **2005**, *67*, 93.
[24] G. Annadurai, L. Y. Ling, J.-F. Lee, *J. Hazard. Mater*. **2008**, *152*, 337.
[25] M. Mukhopadhyay, S. Noronha, G. Suraishkumar, *Can. J. Chem. Eng*. **2011**, *89*, 900.
[26] S.-T. Yang, Y. Chang, H. Wang, G. Liu, S. Chen, Y. Wang, Y. Liu, A. Cao, *J. Colloid Interf. Sci*. **2010**, *35*, 122.
[27] P. Sharma, M. Sharma, R. Tomar, *J. Taiwan Inst. Chem. E.* **2013**, *44*, 480.
[28] M. Barros, I. Araujo, P. Arroyo, E. Sousa-Aguiar, C. Tavares, *Lat. Am. Appl. Res*. **2003**, *33*, 339.
[29] R. Beauchet, J. Mijoin, I. Batonneau-Gener, P. Magnoux, *Appl. Catal. B-Environ.* **2010**, *100*, 91.
[30] R. Beauchet, J. Mijoin, P. Magnoux, *Appl. Catal. B-Environ.* **2009**, *88*, 106.
[31] D. Romero, D. Chlala, M. Labaki, S. Royer, J.-P. Bellat, I. Bezverkhyy, J.-M. Giraudon, J. F. Lamonier, *Catalysts* **2015**, *5*, 1479.
[32] W. Zhao, D. N. Seo, H. S. Kim, H. T. Kim, I. J. Kim, *Asian J. Chem*. **2011**, *23*, 2314.
[33] M. D. Romero, G. Ovejero, A. Rodríguez, J. M. Gómez, *Micropor. Mesopor. Mat.* **2005**, *81*, 313.
[34] H. J. Lee, Y. M. Kim, O. S. Kweon, I. J. Kim, *J. Eur. Ceram. Soc*. **2007**, *27*, 561.

[35] C. W. Purnomo, C. Salim, H. Hinode, *Micropor. Mesopor. Mat.* **2012**, *162*, 6.
[36] X. Zhang, S. Yang, D. Tang, R. Yang, *Mater. Res. Bull.* **2015**, *70*, 343.
[37] M. Batista, M. Morales, E. Baggio-Saitovich, E. Urquieta-Gonzalez, *Hyperfine Interact.* **2001**, *134*, 161.
[38] F. F. Brites-Nóbrega, I. A. Lacerda, S. V. Santos, C. C. Amorim, V. S. Santana, N. R. Fernandes-Machado, J. D. Ardisson, A. B. Henriques, M. M. Leão, *Catal. Today* **2015**, *240*, 168.
[39] L. Singh, P. Rekha, S. Chand, *Sep. Purif. Technol.* **2016**, *170*, 321.
[40] A. Veses, B. Puértolas, M. Callén, T. García, *Micropor. Mesopor. Mat.* **2015**, *209*, 189.
[41] E. F. Iliopoulou, S. Stefanidis, K. Kalogiannis, A. Delimitis, A. Lappas, K. Triantafyllidis, *Appl. Catal. B-Environ.* **2012**, *127*, 281.
[42] W. B. Widayatno, G. Guan, J. Rizkiana, J. Yang, X. Hao, A. Tsutsumi, A. Abudula, *Appl. Catal. B-Environ.* **2016**, *186*, 166.
[43] T. Salama, I. Ali, H. Gumaa, M. Lateef, M. Bakr, *Chemical Sciences Journal* **2016**, *7*, 2150.
[44] S. Jana, S. K. Ghosh, S. Nath, S. Pande, S. Praharaj, S. Panigrahi, S. Basu, T. Endo, T. Pal, *Appl. Catal. A-Gen.* **2006**, *313*, 41.
[45] Y. Zhu, J. Shen, K. Zhou, C. Chen, X. Yang, C. Li, *J. Phys. Chem. C* **2010**, *115*, 1614.
[46] N. Pradhan, A. Pal, T. Pal, *Colloid. Surface. A* **2002**, *196*, 247.
[47] S. Li, S. Guo, H. Yang, G. Gou, R. Ren, J. Li, Z. Dong, J. Jin, J. Ma, *J. Hazard. Mater.* **2014**, *270*, 11.
[48] A. Hatamifard, M. Nasrollahzadeh, S. M. Sajadi, *New J. Chem.* **2016**, *40*, 2501.
[49] Z. M. El-Bahy, *Appl. Catal. A-Gen.* **2013**, *468*, 175.
[50] K. Hayakawa, T. Yoshimura, K. Esumi, *Langmuir* **2003**, *19*, 5517.
[51] P. Zhao, X. Feng, D. Huang, G. Yang, D. Astruc, *Coordin. Chem. Rev.* **2015**, *287*, 144.
[52] A. Shukla, R. K. Singha, T. Sasaki, R. Bal, *Green Chem.* **2015**, *17*, 785.
[53] S. Saha, A. Pal, S. Kundu, S. Basu, T. Pal, *Langmuir* **2009**, *26*, 2885.
[54] W.-J. Liu, K. Tian, H. Jiang, H.-Q. Yu, *Green Chem.* **2014**, *16*, 4198.
[55] K. Layek, M. L. Kantam, M. Shirai, D. Nishio-Hamane, T. Sasaki, H. Maheswaran, *Green Chem.* **2012**, *14*, 3164.
[56] A. Corma, P. Concepción, P. Serna, *Angew. Chem-Ger. Edit.* **2007**, *119*, 7404.
[57] M. Nasrollahzadeh, M. Maham, A. Rostami-Vartooni, M. Bagherzadeh, S. M. Sajadi, *RSC Adv.* **2015**, *5*, 64796.
[58] L. Dou, H. Zhang, *J. Mol. Catal. A-Chem.* **2016**, *4*, 18990.
[59] T. R. Mandlimath, B. Gopal, *J. Mol. Catal. A-Chem.* **2011**, *350*, 9.
[60] A. Hakki, R. Dillert, D. Bahnemann, *Catal. Today* **2009**, *144*, 154.
[61] A. Rostami-Vartooni, M. Alizadeh, M. Bagherzadeh, *Beilstein J. Nanotech.* **2015**, *6*, 2300.
[62] A. Hatamifard, M. Nasrollahzadeh, J. Lipkowski, *RSC Adv.* **2015**, *5*, 2300.
[63] X. Du, J. He, J. Zhu, L. Sun, S. An, *Appl. Surf. Sci.* **2012**, *258*, 92717.
[64] R. Xu, H. Bi, G. He, J. Zhu, H. Chen, *Mater. Res. Bull.* **2014**, *57*, 190.
[65] H. Niu, S. Liu, Y. Cai, F. Wu, X. Zhao, *Micropor. Mesopor. Mat.* **2016**, *219*, 48.
[66] T. Zeng, X. Zhang, S. Wang, Y. Ma, H. Niu, Y. Cai, *J. Mater. Chem.* **2013**, *1*, 11641.
[67] Y. Choi, H. S. Bae, E. Seo, S. Jang, K. H. Park, B.-S. Kim, *J. Mater. Chem.* **2011**, *21*, 15431.
[68] M. Lerma-García, M. Ávila, E. F. Simó-Alfonso, Á. Ríos, M. Zougagh, *Journal of Materials and Environmental Science* **2014**, *5*, 1919.

Table 1: Main ion concentrations in the industrial effluents adopted as catalyst precursor and their pH value

	Species	Conc.		Species	Conc.
Wastewater	pH (30 °C)	6.1	Wastewater	pH (30 °C)	6.5
Effluent-A	SO_4^{-2}	1.8 g/L	Effluent-B	SO_4^{-2}	0.68 g/L
	Zn^{2+}	1.2 mg/L		Zn^{2+}	1.2 mg/L
	Ni^{2+}	0.07 mg/L		Ni^{2+}	0.07 mg/L
	Pb^{2+}	0.2 mg/L		Pb^{2+}	0.2 mg/L
	CN^-	0.15 mg/L		CN^-	0.15 mg/L
	Cd^{2+}	0.05 mg/L		Cd^{2+}	0.05 mg/L
	Cu^{2+}	0.1 mg/L		Cu^{2+}	400 mg/L
	Fe^{3+}	350 mg/L			
	COD	101 mg/L		COD	101 mg/L
	Hg+	0.005 mg/L		Hg+	0.005 mg/L

Table 2: Optimal conditions for the adsorption tests of Fe (III) and Cu (II) over NaX zeolite

	Fe (III)		Cu (II)	
	value	% R	value	% R
pH	3	99.9	3	> 99.9
Contact time (h)	4	98.6	5	98.8
Zeolite NaX loading (g/L)	5	98.7	5	98.0

Table 3: Fe (III) and Cu (II) AAS analysis of wastewater effluents after adsorption over NaX zeolite

	Elements	Concentration (mg/L)	% R
Wastewater (A)	Fe (III)	5	98.5
Wastewater (B)	Cu (II)	8.5	98.0

Table 4: Atomic (At%) and mass (mass%) ratios of zeolites

	NaX		Fe/NaX		Cu/NaX	
	At%	mass%	At%	mass%	At%	mass%
O	56	47	58	42	50	33
Si	18	25	16	20	22	26
Al	13	17	11	14	16	18
Na	10	11	9	9	5	5
Cu					7	18
Fe			6	15		
Si/Al	1.40	1.47	1.46	1.42	1.40	1.44

Table 5: Textural parameters of the catalysts

Sample	S_{BET} (m^2/g)	Average pore diameter (nm)	V_{tot} (cm^3/g)	$V_{micropore}$ (cm^3/g)	$V_{mesopore}$ (cm^3/g)	Meso-/Micropores
NaX	632 ±5	1.9 ±0.1	0.39 ±0.03	0.33 ±0.03	0.06 ±0.02	0.2
Fe/NaX	439 ±4	2.0 ±0.1	0.33 ±0.03	0.15 ±0.02	0.18 ±0.02	1.2
Cu/NaX	314 ±3	2.4 ±0.1	0.20 ±0.02	0.06 ±0.02	0.14 ±0.02	2.3

Table 6: Comparison of catalysts in the reduction of 4-NP

Catalyst	Catalyst loading	p-NP (mol/L)	Reaction time (s) to max conversion	Ref.
Cu NPs/bentonite	15 mg	2.5×10^{-3}	90	Rostami-Vartooni et al. [61]
Ag/zeolite nanocomposite	5 mg	2.5×10^{-3}	160	Hatamifard et al.[48]
Natrolite zeolite/Pd Nanocomposite	7 mg	2.5×10^{-3}	160	Hatamifard et al.[62]
Fe_3O_4-SiO_2–Ag	3 mg	0.005	240	Du et al.[63]
Cu-Fe_3O_4@GE	20 mg	10^{-3}	300	Xu et al.[64]
Cu/Cu_2O/C	0.04 mg	5×10^{-3}	160.2	Niu et al.[65]
SiO_2/Fe_3O_4C/Au	1 mg/ml	5×10^{-3}	200	Zeng et al.[66]
Au–GO	1.4910^{-4} mol/L	7.50×10^{-4}	1500	Choi et al.[67]
AuNPs	10^{-5} mol/L	5.10^{-3}	300	Lerma-García et al.[68]
Fe/NaX	1 mg	5×10^{-3}	100	This work
Cu/NaX	1 mg	5×10^{-3}	60	This work

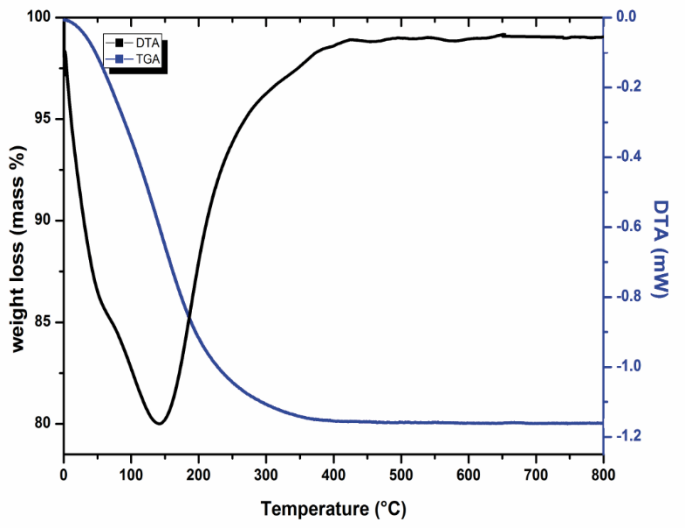

Figure 1

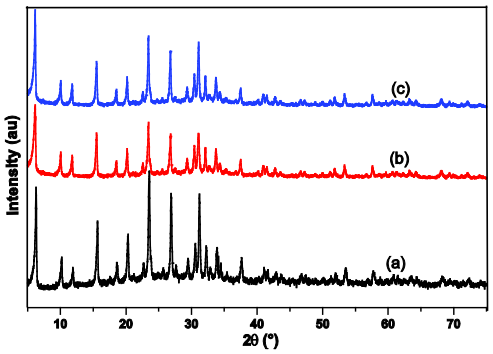

Figure 2

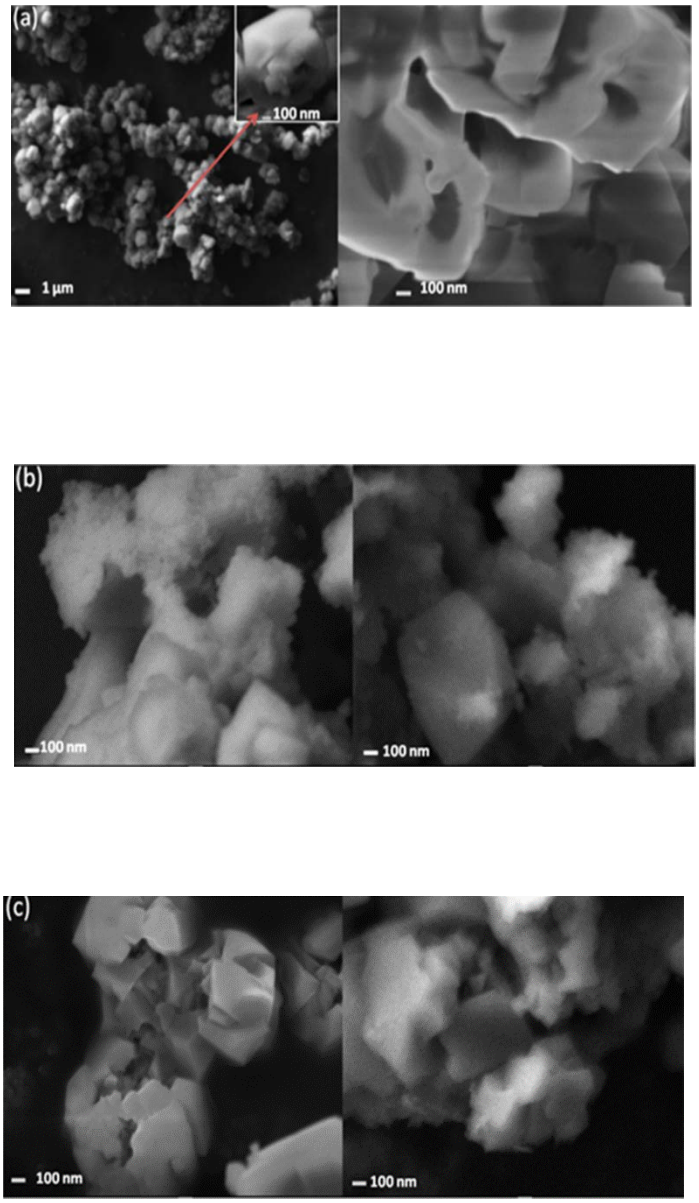

Figure 3

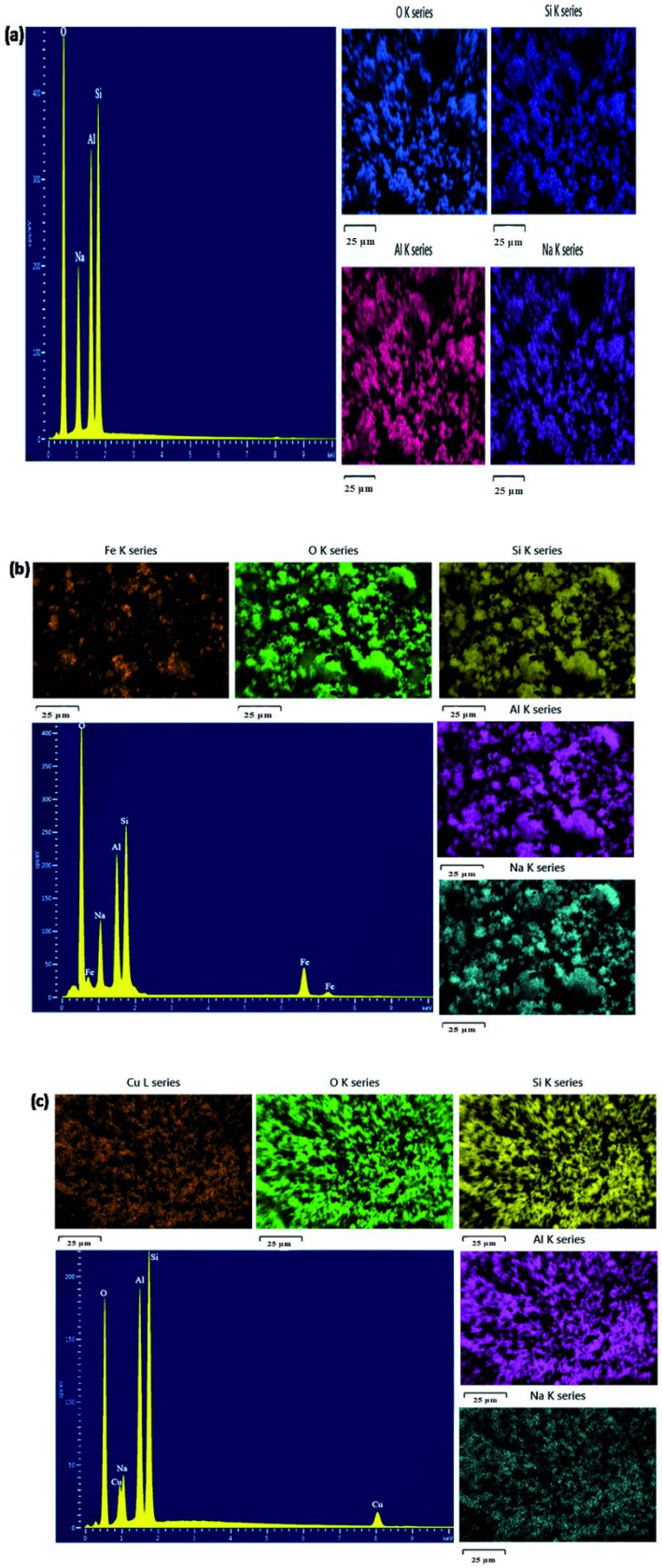

Figure 4

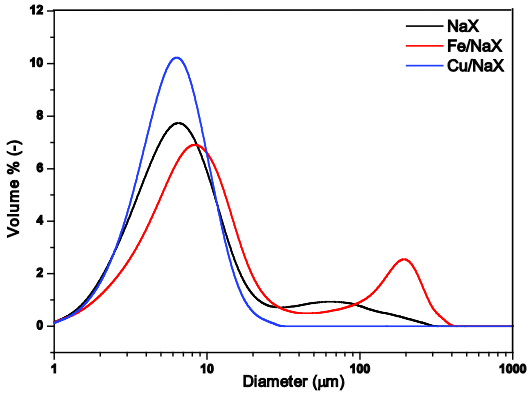

Figure 5

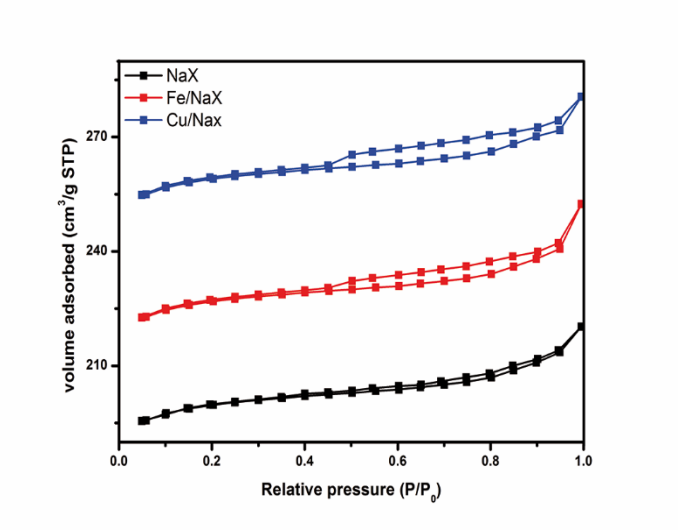

Figure 6

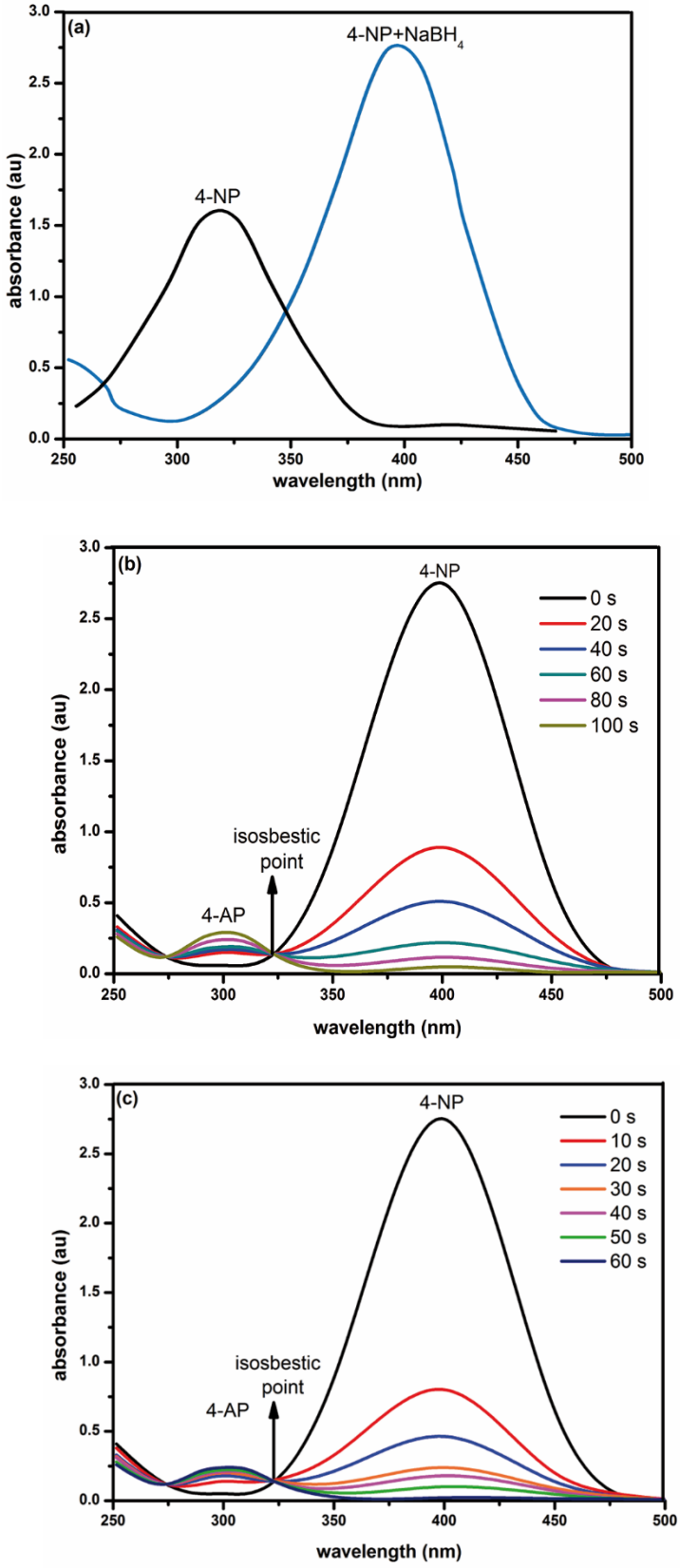

Figure 7

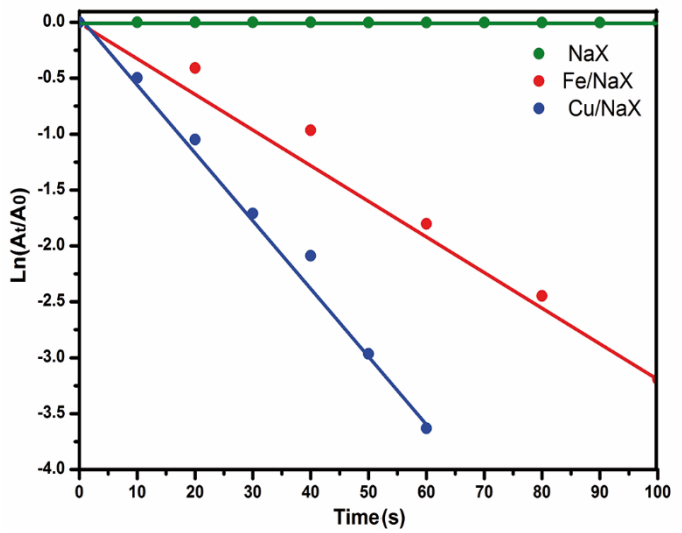

Figure 8

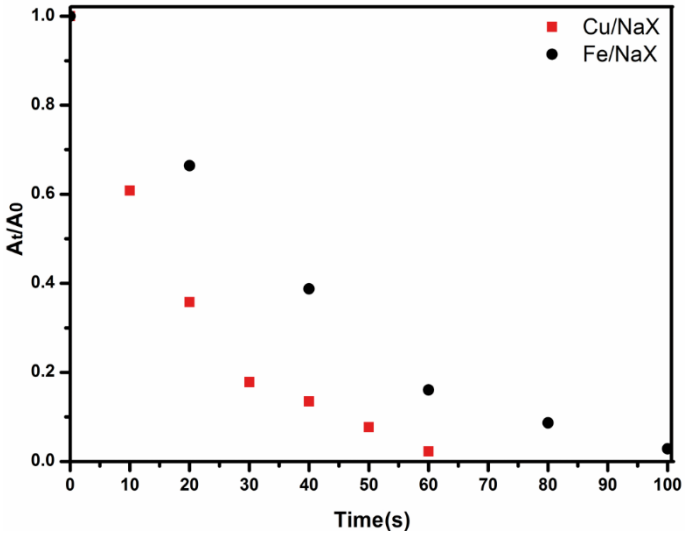

Figure 9

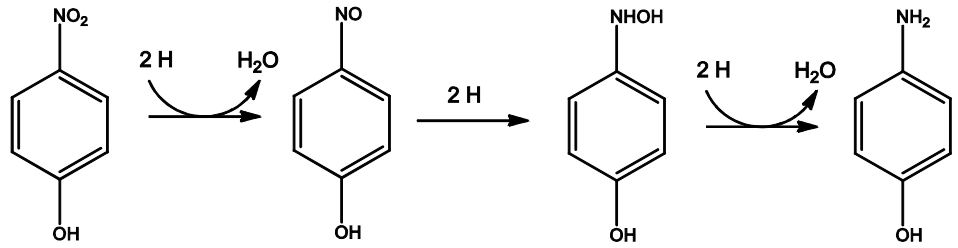

Figure 10

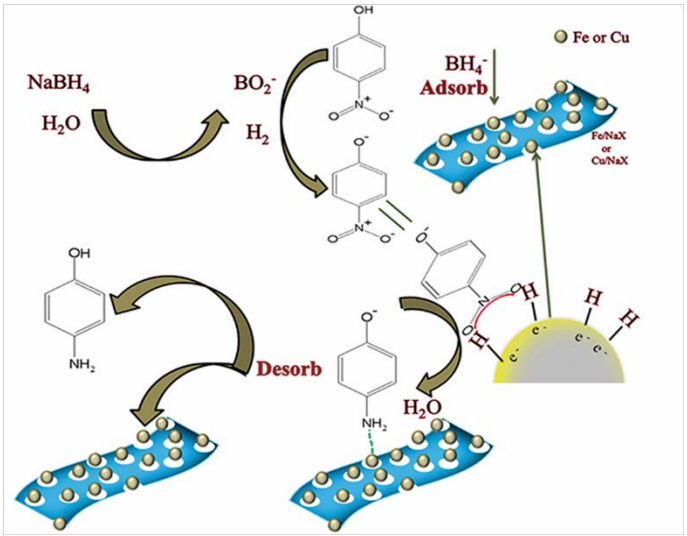

Figure 11

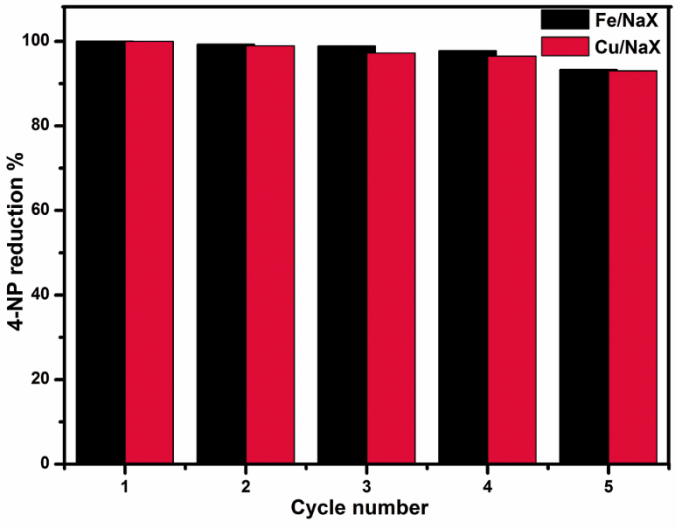

Figure 12